Eur Biophys J (2005) 34: 243–254
DOI 10.1007/s00249-004-0446-8

ARTICLE

Lin Wang · Peng Cai · Hans-Joachim Galla
Huixin He · Carol R. Flach · Richard Mendelsohn

Monolayer–multilayer transitions in a lung surfactant model: IR reflection–absorption spectroscopy and atomic force microscopy

Received: 16 June 2004 / Accepted: 26 October 2004 / Published online: 12 January 2005

Abstract A hydrophobic pulmonary surfactant protein, SP-C, has been implicated in surface-associated activities thought to facilitate the work of breathing. Model surfactant films composed of lipids and SP-C display a reversible transition from a monolayer to surface-associated multilayers upon compression and expansion at the air/water (A/W) interface. The molecular-level mechanics of this process are not yet fully understood. The current work uses atomic force microscopy on Langmuir–Blodgett films to verify the formation of multilayers in a dipalmitoylphosphatidylcholine, dipalmitoylphosphatidylglycerol, cholesterol, and SP-C model system. Isotherms of SP-C-containing films are consistent with exclusion and essentially complete respreading during compression and expansion, respectively. Multilayer formation was not detected in the absence of SP-C. Most notable are the results from IR reflection–absorption spectroscopy (IRRAS) conducted at the A/W interface, where the position and intensity of the Amide I band of SP-C reveal that the predominantly helical structure changes its orientation in monolayers versus multilayers. IRRAS measurements indicate that the helix tilt angle changed from approximately 80° in monolayers to a transmembrane orientation in multilayers. The results constitute the first quantitative measure of helix orientation in mixed monolayer/multilamellar domains at the A/W interface and provide insight into the molecular mechanism for SP-C-facilitated respreading of surfactant.

Keywords Pulmonary surfactant · Surfactant protein SP-C · Helix tilt angle · Surface-associated reservoir

L. Wang · P. Cai · H. He · C. R. Flach (✉) · R. Mendelsohn
Department of Chemistry, Newark College of Arts and Sciences, Rutgers University, 73 Warren Street, Newark, NJ 07102, USA
E-mail: flach@andromeda.rutgers.edu
Tel.: +1-973-3531330
Fax: +1-973-3531264

H.-J. Galla
Institut für Biochemie, Westfälische Wilhelms-Universität, 48149 Münster, Germany

Abbreviations AFM: Atomic force microscopy · ATR: Attenuated total reflectance · A/W: Air/water · DLigPC: 1,2-Dilignoceroyl phosphatidylcholine · DPPC: 1,2-Dipalmitoylphosphatidylcholine · DPPG: 1,2-Dipalmitoylphosphatidylglycerol · DSPC: 1,2-Distearoylphosphatidylcholine · EDTA: Ethylenediaminetetraacetate · IRRAS: IR reflection–absorption spectroscopy · LB: Langmuir–Blodgett · PC: Phosphatidylcholine · PG: Phosphatidylglycerol · $\pi-A$: Surface pressure–molecular area · POPG: 1-Palmitoyl-2-oleoyl phosphatidylglycerol · SFM: Scanning force microscopy · TOF-SIMS: Time-of-flight secondary ion mass spectrometry · Tris: Tris(hydroxymethyl)aminomethane

Introduction

Pulmonary surfactant is a lipid/protein complex located at the air/alveolar lining of the mammalian lung. It functions in vivo to prevent alveolar collapse during exhalation by lowering surface tension to near-zero values. Pulmonary surfactant lipids (90% by weight) contain mainly 1,2-dipalmitoylphosphatidylcholine (DPPC) and phosphatidylglycerols (PGs) along with a significant proportion of unsaturated phosphatidylcholines (PCs) and PGs, other phospholipid classes, and cholesterol. There are four surfactant-associated proteins, SP-A, SP-B, SP-C, and SP-D, of which two, SP-B and SP-C, are very hydrophobic and are implicated in controlling the surface properties of surfactant. In particular these proteins have been shown to facilitate the spreading of lipids across air/water (A/W) interfaces.

Surfactant in vivo must possess two apparently contradictory attributes. It must be able to form stable films at the high surface pressures (approximately 70 mN m^{-1}) that form upon exhalation; and it must also be able to spread sufficiently rapidly across the air/alveolar interface to keep up with breathing rates. At the interface, lung surfactant has been presumed to exist as a

monolayer, although this basic tenet has recently been questioned. DPPC is the major surfactant constituent that can form stable monolayers at 70 mN m^{-1} under compressive forces; however, it spreads too slowly during surface area expansion to be effective in vivo. To address this issue, Goerke and Clements (1986) proposed that for films to be stable, a process had to occur during which the surface concentration of DPPC was enhanced at high pressures. The process, not defined in molecular structure terms, was labeled "squeeze-out", and alluded to a concentrating of the DPPC in the surface film upon compression. About a decade ago, we observed this phenomenon at high pressures in binary lipid mixtures such as DPPC/1-palmitoyl-2-oleoyl phosphatidylglycerol (POPG) (Pastrana-Rios et al. 1994) in which one component (e.g., the POPG) was more structurally disordered and more likely to be unstable in monolayers at high surface pressures (π).

The deficiency in the model of surfactant action as then propounded was that the mechanism of surfactant respreading was not addressed. Recent data, both from intact lung and from transferred films, have suggested that surface-associated multilayers form at high π values during expansion–contraction cycles. Schürch et al. (1998) used electron microscopy of guinea pig lungs to observe multilayer structures with variations in the number of lamellae from 2 to 7. To characterize similar structures in surface films formed from synthetic phospholipids (DPPC, 1,2-dipalmitoylphosphatidylglycerol, DPPG) and recombinant SP-C, von Nahmen et al. (1997) used scanning force microscopy (SFM) to search for multilayers at high pressures. The images confirmed the presence of multilayers in the late stages of compression. Step heights within the protrusions were slightly larger than a DPPC bilayer in the gel phase (approximately 55–65 Å). π–molecular area (π–A) isotherms suggested that the excluded material remained associated with the monolayer on compression and respread into the monolayer upon expansion. Takamoto et al. (2001), using fluorescence and atomic force microscopy (AFM), noted that synthetic SP-B and a deacylated analogue of SP-C (in separate experiments) induced a two- to three-dimensional transformation of the fluid phase fraction in mixed DPPG/POPG monolayers. The transition was found to be reversible in the presence of SP-B. These results suggest that the excluded material remains near the interface at high pressure, leading to the proposition that surfactant may exist in two physical states at the air/alveolar lining.

Additional studies of multilayer formation have probed the roles of specific lipids and various combinations or concentrations of surfactant proteins or peptide analogues (Bourdos et al. 2000; Diemel et al. 2002b; Krol et al. 2000). In particular, studies using time-of-flight secondary ion mass spectrometry (TOF-SIMS) of Langmuir–Blodgett (LB) films reveal domain structures in DPPG/SP-C films but not in DPPC/SP-C films (Bourdos et al. 2000). The domain structures appear to be correlated with the ability to form stable collapse structures, i.e., multilayers. These and earlier TOF-SIMS studies on DPPC/DPPG/SP-C films correlated with fluorescence microscopy and SFM suggested that SP-C enrichment occurs in the multilayer regions and that some DPPC is also present in the multilayers (Bourdos et al. 2000; Galla et al. 1998). AFM studies of model systems containing SP-B have shown that the multilayer protrusion height depends on whether the lipids contain an unsaturated acyl chain and whether this unsaturated chain is present in the PC or PG lipid constituent (Diemel et al. 2002b). Cholesterol also appears to play a role by promoting the homogeneous distribution of the protrusions in one particular model system (Diemel et al. 2002a). In summary, SP-B, SP-C, and the presence of PG lipids have been implicated in the reversible formation of a surface-associated reservoir at high pressures from which respreading occurs upon expansion.

Although the techniques just cited provide the spatial resolution to detect multilayer states and TOF-SIMS provides important additional information revealing the spatially resolved relative concentrations of the chemical constituents, the methods do not provide molecular structure information. An understanding of the molecular properties of the film constituents will guide the design of therapeutic agents for pathological lung states such as respiratory distress syndrome.

The current study uses IR reflection–absorption spectroscopy (IRRAS) to directly monitor the secondary structure and orientation of native, porcine SP-C in mixed monolayers and multilayers at the A/W interface with DPPC, DPPG, and cholesterol. SP-C is a 4.2-kDa lipoprotein with a very regular, valine-rich α-helical structure (residues 9–34) as determined by NMR in organic solvent (Johansson et al. 1994). Two cysteine residues at positions 5 and 6 are palmitoylated via thioester linkages in porcine and human variants. The N-terminus also has three positively charged residues. The balance between the charged residues and the acylation is thought to provide some flexibility and stability to the N-terminus in interfacial environments (Bi et al. 2002; Plasencia et al. 2001), while the hydrophobic helical region has a transmembrane orientation in lipid bilayers (Pastrana et al. 1991). Although SP-C-deficient mice survive, lung mechanics studies demonstrated abnormalities and a significant decrease in stability was observed in captive bubbles formed with surfactant from the knockout mice (Glasser et al. 2001).

IRRAS is currently the only physical method able to directly monitor peptide secondary structure in situ in Langmuir films. Since the IRRAS measurement is macroscopic in nature, even though it directly monitors molecular conformation, we have used AFM on transferred films to verify the formation of multilayers in this system, as well as π–A isotherms to characterize surface thermodynamics. AFM provides the opportunity to monitor the surface nanostructure of these films at high resolution. Taken together, these techniques provide compelling confirmation of a monolayer-to-multilayer

transition either enhanced or induced by SP-C, with additional information being gleaned about the secondary structure and orientation of the SP-C in both monolayers and multilayers.

Materials and methods

Materials

The required amounts of DPPC, DPPG, 1,2-distearoylphosphatidylcholine (DSPC), and 1,2-dilignoceroyl phosphatidylcholine (DLigPC) were purchased from Avanti Polar Lipids (Alabaster, AL, USA) and were used without further purification. Chloroform, methanol, ethylenediaminetetraacetate (EDTA), and high-performance liquid chromatography grade water were obtained from Fisher Scientific (Pittsburgh, PA, USA). Tris(hydroxymethyl)aminomethane (Tris) hydrochloride, Tris base (Trizma), cholesterol, and sodium chloride were purchased from Sigma (St. Louis, MO, USA). D_2O with 99.9% isotopic enrichment was purchased from Cambridge Isotope Laboratories (Andover, MA, USA). Highly purified porcine SP-C (S-palmitoylated) was a generous gift of Kevin Keough (Memorial University of Newfoundland).

Methods

Sample preparation

PC lipids, cholesterol, and SP-C stock solutions were prepared in chloroform, while DPPG was dissolved in chloroform/methanol (4/1, v/v) at approximately 1 mg ml^{-1} concentration. The sample solutions were prepared by mixing the stock solutions in various proportions to obtain the desired ratio of components. A DSPC/DLigPC solution (1/1 molar ratio) and model surfactant solutions consisting of DPPC/DPPG at a 4/1 molar ratio with 7 mol% cholesterol with or without 4 mol% SP-C were prepared.

Isotherm acquisition and LB transfer

π–A isotherms were acquired with a Nima Technology (Coventry, UK) model 611 LB trough (maximum surface area of approximately 600 cm^2) with a model PS4 surface-pressure sensor based on a paper Wilhelmy plate. The trough was equipped with a D1L-75 standard linear dipper. The subphase consisted of either pure high-performance liquid chromatography water for the DSPC/DLigPC experiments or 100 mM NaCl and 0.1 mM EDTA in 5 mM Tris buffer at pH 7 for all other experiments. The subphase temperature was held at 20°C. When LB films were being transferred, a freshly cleaved mica sheet (Agar Scientific, Essex, UK) was submerged into the subphase, prior to spreading the film. Typically, 25–30 µl of solution was spread dropwise onto the surface and 20–30 min was allowed for solvent evaporation prior to compression. Films were compressed and, in particular experiments, expanded at a speed of approximately 0.05 nm^2 per lipid molecule per minute. For LB transfer from isotherm regions not displaying a plateau, pressure control was applied as the target pressure was approached and a further 10-min equilibration time was permitted. Films were then transferred onto the mica at a rate of 5 mm min^{-1} using pressure control. For the SP-C-containing films in the plateau region of the isotherm ($\pi \sim 55$ mN m^{-1}), the barrier was stopped for a 10-min equilibration period followed by transfer at constant area.

AFM measurements

The AFM measurements were performed using a multimode AFM (Nanoscope IIIa; Digital Instruments, Santa Barbara, CA, USA). Tapping mode topographic images were taken (J-type scanner with a 125-×125-µm scan range) in air using silicon NanoProbe tips (OTESPA) with a resonance frequency of approximately 300 kHz, a spring constant of approximately 42 N m^{-1}, and a tip radius of less than 10 nm. Scan rates varied from 0.6 to 0.85 Hz and the ratio of setpoint amplitude to vibration amplitude ranged from 0.4 to 0.9. Height differences were obtained from section analysis of the topographic images. In the topographic images, variations in height are shown using a grayscale gradient with the lightest color being the highest point in the image.

IRRAS measurements and data analysis

The IRRAS spectra were acquired with a Bruker Instruments Equinox 55 spectrometer equipped with an external variable-angle reflectance accessory, the XA511. The accessory is coupled to a custom-designed Langmuir trough constructed by Nima Technology (Coventry, UK) equipped with a Nima model PS4 surface pressure sensor. The instrument has been described elsewhere (Flach et al. 2001). Briefly, the IR beam is directed through the external port in the spectrometer and is reflected by three mirrors in a rigid mount prior to being focused on the water surface. Computer-driven stepper motors rotate the mirrors to obtain the desired angle of incidence. A wire grid polarizer is placed into the optical path directly before the beam impinges on the water surface. The reflected light is collected at the same angle as the angle of incidence, follows an equivalent mirror path, and is directed onto a narrow-band mercury/cadmium telluride detector. The entire experimental setup is enclosed and purged to keep the relative humidity levels both low and as constant as feasible.

A D_2O-based subphase consisting of 100 mM NaCl and 0.1 mM EDTA in 5 mM Tris buffer at pD 7 was used for all IRRAS experiments. A D_2O-based subphase is used to eliminate the reflectance–absorbance from the

(liquid) H_2O-bending vibration and to lessen the absorbance from the rotation–vibration bands of water vapor, both of which occur in the conformation-sensitive Amide I spectral region. The subphase temperature was thermostated at 21.0 ± 0.5°C. Aliquots of the sample solutions (approximately 10 μl) were spread dropwise on a clean surface (maximum surface area of 86 cm^2). A minimum of 40 min was allowed for solvent evaporation and film relaxation/equilibration prior to compression. Samples were spread with initial pressure values ranging from 2–8 mN m^{-1} and π–A isotherms were acquired during intermittent compression. IRRAS spectral acquisition was conducted 5 min after the stopping of the barrier at the desired surface pressure. The surface pressure drop during IRRAS measurements was less than 5 mN m^{-1} in high-pressure regions (approximately 50 mN m^{-1}) and less than 2 mN m^{-1} in low-pressure regions (approximately 25 mN m^{-1}). Spectra of the films were acquired under conditions of both film expansion and film compression. Measured spectral parameters acquired following film expansion were quite sensitive to the details of the compression and expansion process. This point is elaborated upon in the Discussion.

Interferograms were collected with a sample shuttle program to compensate for the residual water vapor rotation–vibration bands. In total 2,048 scans were acquired at 8-cm^{-1} resolution in eight blocks of 256 scans each for p polarization and 1,024 scans were acquired at 8-cm^{-1} resolution in four blocks of 256 scans each for s-polarization, coadded, apodized with a Blackman Harris three-term function, and fast Fourier-transformed with two levels of zero filling to produce spectral data encoded at approximately 2-cm^{-1} intervals. Spectra were acquired at various angles of incidence, typically ranging from 34° to 47°.

Data analysis was performed using Grams/32 software (Galactic Industries Corp., Salem, NH, USA). The spectra were presented and peak heights for the Amide I band were determined after baseline correction. The excellent spectral quality and compensation of water vapor precluded the need for water vapor subtraction. The resulting Amide I peak heights were used to determine the orientation of the helical region of SP-C. Peak positions were determined using a center-of-gravity algorithm provided by the National Research Council of Canada.

IRRAS simulations

The dependence of the Amide I band intensity for both s- and p-polarized radiation on the incident angle is used to determine the orientation of the helical region in SP-C (average helix tilt angle with respect to the surface normal). The methods have been previously described (Brauner et al. 2003; Flach et al. 1997; Gericke et al. 1997). Briefly, the optical theory of Kuzmin and associates (Kuzmin and Michailov 1981; Kuzmin et al. 1992) was applied, which requires knowledge of the subphase and monolayer optical constants, i.e., the real and imaginary parts of the refractive index. Values for D_2O are obtained from Bertie et al. (1989). The real part of the refractive index for the monolayer has been obtained from IR ellipsometric measurements (A. Roseler, unpublished results) and is assumed to be isotropic. The imaginary part of the refractive index for the monolayer (referred to as the scale factor in the calculations) is related to the extinction coefficient for the vibrational mode. The strong dependence of the calculated intensities on the scale factor is lessened by employing a standard technique used in attenuated total reflectance (ATR) IR spectroscopy, namely, the use of dichroic ratios (p-polarized to s-polarized intensity ratio) (Brauner et al. 2003). Use of dichroic ratios also reduces the dependence of the calculated intensities on film thickness. The directional components for the scale factor are calculated using Fraser's model for uniaxial symmetry (Fraser and MacRae 1973). The model also requires the angle between the helix axis and the transition dipole moment direction as an input and this was taken as 28° (Rothschild and Clark 1979). Dichroic ratios were calculated for a variety of tilt angles over a range of incident angles and were compared with experimentally measured ratios to determine the helix tilt. In recent work (Brauner et al. 2003), we have extended the model to allow for deviations from uniaxial symmetry. This extended model was required to calculate the tilt angles of acyl chains in ordered phases at surface pressures of 40 mN m^{-1} and above.

Results

Isotherms and AFM measurements of LB films

The AFM measurements were conducted on LB films of binary lipid monolayers consisting of DSPC/DLigPC (1/1 molar ratio) to assess the sensitivity and accuracy of the LB transfer process and AFM measurements. Figure 1a displays an isotherm of the mixed lipid monolayer, where the arrow marks the pressure (30 mN m^{-1}) at which film transfer took place. The shape of the isotherm is typical of a condensed monolayer consistent with the fact that in the bulk phase both lipids are in an ordered (gel) state at room temperature. The inset in Fig. 1a shows the AFM topography (10×10 μm^2) of the LB film, with Fig. 1b depicting the height variations along the line drawn in the image. The height difference between the two small arrowheads marked on the line plot (0.78 nm) is representative of the majority of the variation in the image and is remarkably close to the value calculated for the chain-length difference (six carbons) between the two lipids with acyl chains in the all-*trans* conformation (0.76 nm). This strongly suggests that the lighter domains in the AFM image predominantly consist of the longer chain lipid, DLigPC, with the darker areas composed of primarily DSPC. Previously reported bulk-phase FTIR measurements

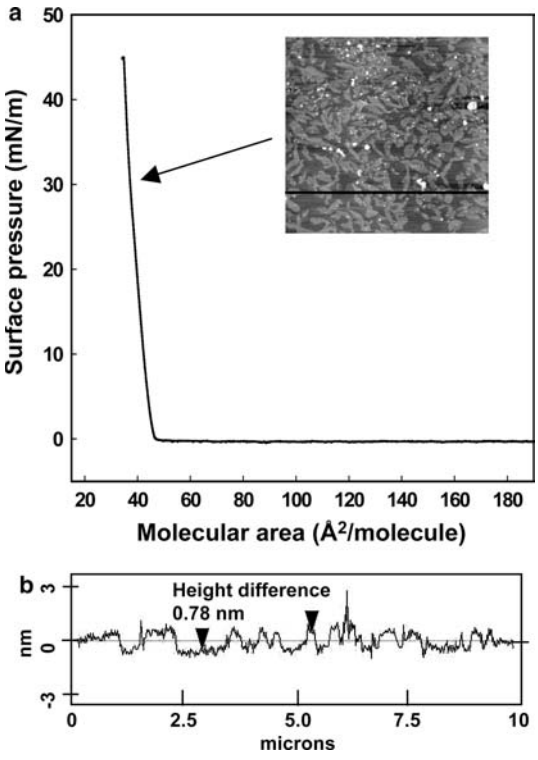

Fig. 1 **a** Surface pressure–molecular area (π–*A*) isotherm of a 1,2-distearoylphosphatidylcholine/1,2-dilignoceroyl phosphatidylcholine (equimolar) monolayer on a water subphase. The *arrow* shows the position on the isotherm ($\pi = 30$ mN m^{-1}) at which the film was transferred onto a mica substrate. The *inset* depicts the atomic force microscopy (*AFM*) topography (10×10 μm^2) of the monolayer with height differences along the line drawn in the image shown in **b**. The majority of the height variation in the image is approximately 0.8 nm and is attributed to the difference in the all-*trans* acyl chain length for the two lipids

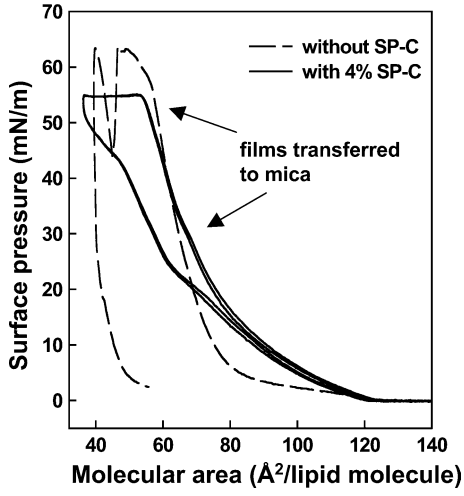

Fig. 2 π–*A* isotherms of a 1,2-dipalmitoylphosphatidylcholine (*DPPC*)/1,2-dipalmitoylphosphatidylglycerol (*DPPG*)/cholesterol (4/1 molar ratio with 7 mol% cholesterol) monolayer in the absence (*dashed line*) and presence (*solid lines*) of 4 mol% native porcine SP-C on a buffered subphase, pH 7, containing 100 mN NaCl and 0.1 mM ethylenediaminetetraacetate (*EDTA*). The lipid monolayer in the absence of SP-C collapses at $\pi \sim 63$ mN m^{-1}, whereas an exclusion plateau is formed at $\pi \sim 55$ mN m^{-1} in the presence of SP-C. The four-component film was compressed and expanded twice. Retracing of the isotherm upon the second compression and expansion indicates that essentially all of the excluded material is reinserted into the monolayer upon expansion. The *arrows* mark the pressure values at which films were transferred to mica supports for AFM measurements

for these two lipids (Mendelsohn et al. 1995) are consistent with the phase separation visualized here.

π–*A* isotherms of the three-component lipid mixture (DPPC/DPPG/cholesterol) with and without SP-C on a buffered water subphase acquired at 21°C are shown in Fig. 2. The obvious plateau observed in the isotherm in the presence of SP-C at $\pi \sim 55$ mN m^{-1} indicates exclusion of material from the surface. The transition is reversible, i.e., a complete reinsertion of excluded material takes place upon expansion in the four-component system as indicated by the retracing of the isotherm upon a second compression. The abrupt dip in the isotherm (at approximately 45 Å^2 per lipid molecule) for the lipid mixture in the absence of SP-C indicates either film leakage or monolayer collapse at $\pi \geq 60$ mN m^{-1} with irreversible loss of film components. The arrows mark the pressure values (30 and 55 mN m^{-1}) at which films, for each sample, were transferred onto freshly cleaved mica for AFM measurements. Films were transferred from the center of the plateau region for the SP-C-containing sample at $\pi = 55$ mN m^{-1} as shown in Fig. 2.

Representative AFM topography (10×10 μm^2) for the two films, each at $\pi \sim 30$ and 55 mN m^{-1}, are shown in Fig. 3a–d, with height variation plots depicted underneath for the lines drawn in each image. The *z*-scale bar shown to the right of Fig. 3a applies to the first three images, while Fig. 3d needed an expanded scale to accommodate the larger height differences observed. It is immediately evident on comparing the overall AFM topography and the line plots that only in Fig. 3d, i.e., in the presence of SP-C and at high surface pressures (55 mN m^{-1}), do we see the significant formation of multilayers. The smallest height variation (less than 1 nm) is observed for the film in the absence of SP-C transferred at $\pi \sim 30$ mN m^{-1} (Fig. 3a). The appearance of a relatively small number of domains with a height difference close to that of a single DPPC bilayer in the gel state (Marsh 1990) is observed for the film in the absence of SP-C (4.7 ± 0.3 nm) as the surface pressure approaches that of collapse (Fig. 3b).

Representative AFM images of the SP-C-containing film clearly differ from the three-component lipid images (Fig. 3c, d compared with a, b, respectively). For the SP-C-containing film transferred at the lower pressure (Fig. 3c), quite a few small protrusions (lightest gray/white) are evident among a background that contains several regions with a fine filamentous appearance. The heights of the majority of the protrusions vary from 1 to less than 5 nm and these small structures are suggested to be nucleation sites for subsequent multilayer formation. Similar height variations and a filamentous appearance were previously reported for a DPPC/

DPPG/SP-C (lipid molar ratio 4/1, protein content 0.4 mol%) LB film (Krol et al. 2000). In marked contrast, a network of bright domain structures is observed in the AFM image (Fig. 3d) of the protein-containing film transferred in the plateau region of the compression isotherm. A variety of heights for the protrusions are shown in the line plot underneath the image. The majority of the height variation shown in the line plot appears to be in multiples of approximately 4.0 nm, possibly representing bilayer stacks. Slight deviations from strict multiples of bilayer thickness, as seen here and in previous reports (Diemel et al. 2002b; Galla et al. 1998), may arise from both uncertainties in the area occupied by SP-C in the *z*-direction and experimental artifacts, including possible film compression or smearing by the AFM tip. The flat areas shown in the darkest color in the image and as the "baseline" in the line plot may be the result of the probe tip sampling the monolayer that was originally formed at the A/W interface. Height variations in these areas are generally less than 1 nm. It must also be noted that the AFM images do not allow us to differentiate whether the multilayers are initially formed above or below the air/monolayer interface, although a previous SFM study conducted at the A/W interface of a bubble reports that the protrusions are predominantly oriented towards the aqueous phase (Knebel et al. 2002). The network of domain structures or protrusions in the *x*–*y* plane shown in Fig. 3d has been previously reported for both SP-C- and SP-B-containing LB films (Diemel et al. 2002b; Krol et al. 2000; von Nahmen et al. 1997). A few of the bigger protrusions reach heights as large as 200 nm. These are most likely due to the "static" nature of our experiment where during the equilibration period, which allows for film stabilization at the A/W interface before transferring to the mica supports, multilayers consisting of a higher number of bilayers may form.

IRRAS of lipid/SP-C monolayers in situ

The IRRAS spectra were acquired from lipid/protein films (DPPC/DPPG 4/1 molar ratio with 7 mol% cholesterol and 4 mol% SP-C) using *s*- and *p*-polarized

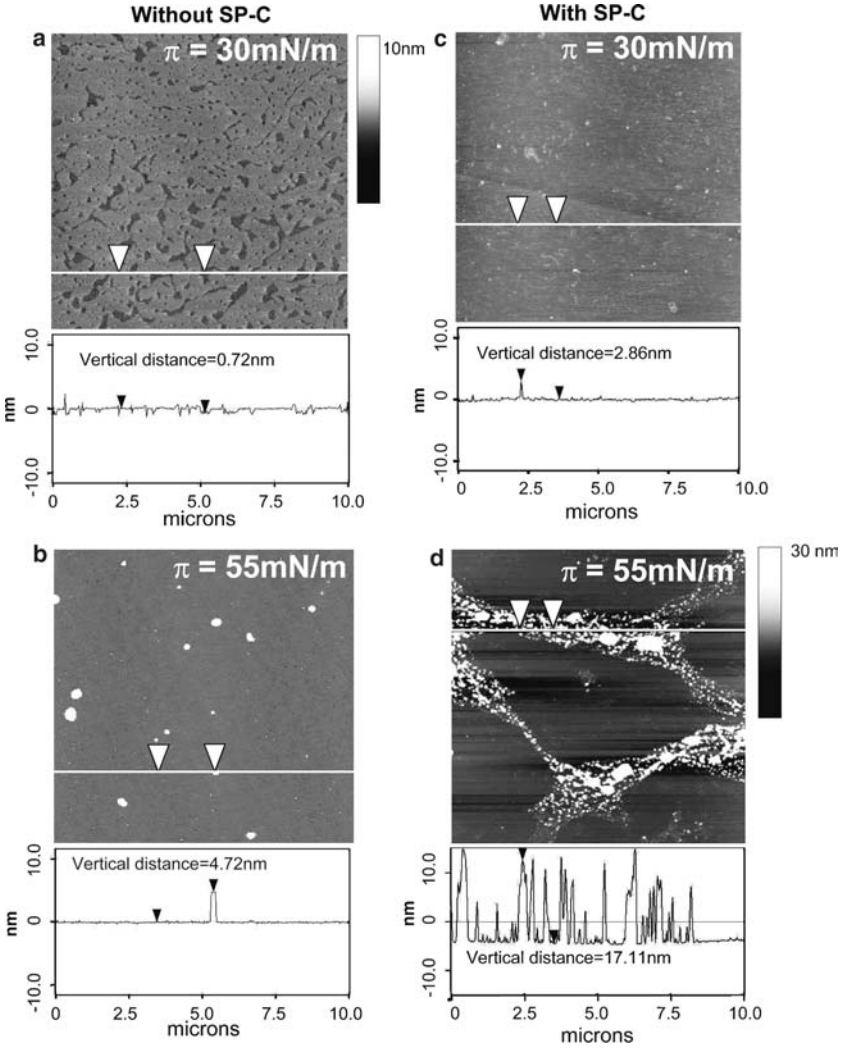

Fig. 3 AFM topographic images of DPPC/DPPG/cholesterol (4/1 molar ratio with 7 mol% cholesterol) films in the presence and absence of 4 mol% SP-C transferred onto mica at two different pressure values as noted. The *10-nm scale bar* shown to the *right* of **a** applies to **a**–**c** and the *30-nm scale bar* applies to **d**. The height variation along the line drawn in each image is shown underneath each respective image. *Arrowheads* in the images and line plots correspond to the same locations for each film, respectively. A smaller scale is used for the images compared with the line plots in **a**–**c** to allow for better contrast in the images. Multilayer formation is apparent for the SP-C-containing film transferred in the plateau region ($\pi = 55$ mN m^{-1}) as shown in **d**

radiation at various surface pressures (25, 40, and 55 mN m^{-1}) and at several angles of incidence. Spectra were collected in either the compression mode or the expansion mode. The compression mode refers to an experimental protocol where spectral acquisition took place at relatively low pressure values prior to collection in the plateau region. In the expansion mode, the film was directly compressed to a pressure within the plateau. Spectra were then acquired, followed by film expansion and data acquisition at $\pi = 25$ mN m^{-1}. A total of approximately 20 IRRAS experiments were conducted. In addition, at $\pi = 55$ mN m^{-1}, the length of the plateau region (Fig. 2) varied from approximately 15 to approximately 30 Å ^{2} per lipid molecule between samples. Typical IRRAS spectra of the Amide I and lipid carbonyl regions acquired using the expansion mode, plateau length approximately 15 Å ^{2} per lipid molecule, are shown in Fig. 4. The Amide I band position, observed at approximately 1,650 cm^{-1}, is indicative of predominantly helical structure at all pressures. This secondary structure was basically unchanged in all experiments. For spectra acquired at higher pressures, (Fig. 4c, d), the Amide I peak is observed to shift up in frequency by approximately 3 cm^{-1}, while the band appears a bit more asymmetric compared with that at lower pressures with a slight increase in intensity on the low-frequency side.

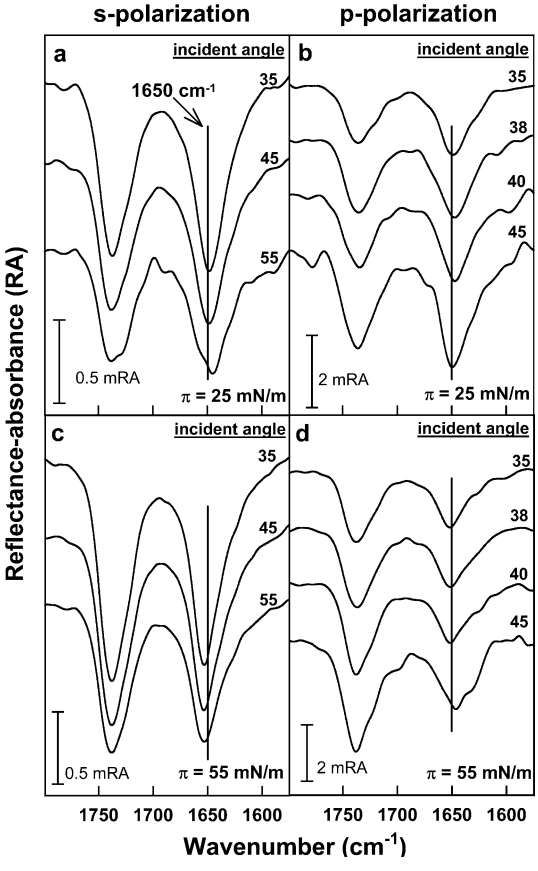

Fig. 4 The IR reflection–absorption spectroscopy (*IRRAS*) spectra (1,800–1,575 cm^{-1}) of a DPPC/DPPG/cholesterol (4/1 molar ratio with 7 mol% cholesterol) film in the presence of 4 mol% SP-C acquired using *s*- and *p*-polarized radiation over a range of incident angles at $\pi = 25$ mN m^{-1} (**a**, **b**) and $\pi = 55$ mN m^{-1} (**c**, **d**). A D_2O-buffered subphase, pD 7, with 100 mM NaCl and 0.1 mM EDTA was used. The lipid carbonyl stretching mode is observed at approximately 1,735 cm^{-1} and the protein Amide I mode is evident at approximately 1,650 cm^{-1}. A *vertical line* is drawn at 1,650 cm^{-1} in each panel to highlight the increase in frequency for the Amide I band at high pressure (compare band positions in **a** and **c** and in **b** and **d**)

Evaluating the dependence of the Amide I band intensity for both *s*- and *p*-polarized radiation on incident angle is necessary for determination of the orientation of the helical region in SP-C (average helix tilt angle with respect to the surface normal). The Amide I band in the spectra acquired using *s*-polarized radiation shows an intensity decrease with an increase in the angle of incidence for each pressure value (Fig. 4a, c). The degree of intensity variation with incident angle for the *p*-polarized spectra is different for each pressure value. For the IRRAS spectra acquired at $\pi = 25$ mN m^{-1} (Fig. 4b), the Amide I band intensity is observed to increase with increasing incident angle, whereas very little change in intensity is observed for the spectra acquired at $\pi = 55$ mN m^{-1} (Fig. 4d). This suggests different orientations of SP-C at the two pressures.

In Fig. 5, the experimentally measured dichroic ratios for the Amide I band over a range of incident angles at π values of 25, 40, and 55 mN m^{-1} are compared with simulated values. Data are shown for films compressed from high areas per molecule, i.e., compression mode, averaged from several experiments (experimental data shown as individual symbols). Dichroic ratios simulated for an 80° helix tilt angle are shown as a solid line and provide an excellent fit for the data acquired at pressures of both 25 and 40 mN m^{-1}. No significant differences in helix tilts are observed between these two surface pressures. The value of 80° is slightly higher than the tilt angle (70°) reported previously for mixed DPPC/SP-C monolayers at $\pi = 28$ mN m^{-1} (Gericke et al. 1997). It is noted that spectra collected in the expansion mode (i.e., films re-expanded to π values of 25 mN m^{-1} following compression to the plateau region) show tilt angles dependent on the detailed experimental conditions. These data, depicted in Fig. 7, are discussed later.

Also evident in Fig. 5 is a marked decrease in the experimental dichroic ratios as a function of incident angle for experiments conducted at $\pi = 55$ mN m^{-1}. Two approaches can be reasonably envisioned to explain the high-pressure IRRAS data. These are essentially a ''one-state'' and a ''two-state'' model.

The one-state model assumes that protein orientation in the film is essentially homogeneous, and thus requires the data to be fit to a dichroic ratio curve calculated using a single tilt angle, as shown in Fig. 5 for calculated values using a tilt angle of 50°. Reasonable agreement between experimental and simulated intensities is achieved with this approach. However, the experimental evidence suggests that a two-state model is equally or

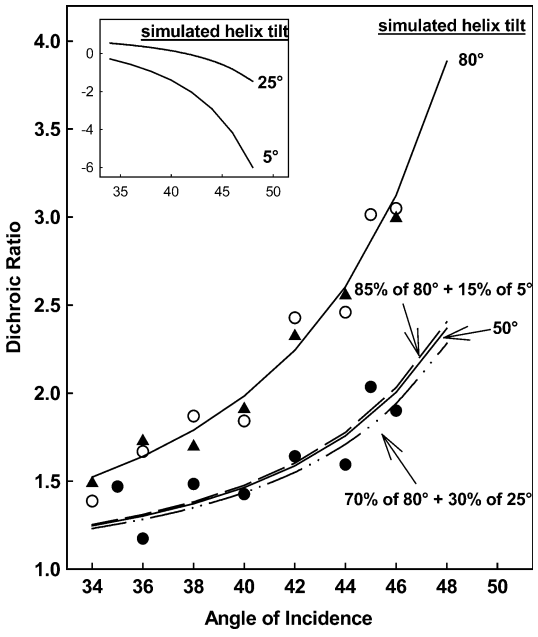

Fig. 5 Dichroic ratio (*p*-polarized to *s*-polarized Amide I band intensity) versus angle of incidence for experimental data (average of 2–5 experiments) acquired using the compression mode at $\pi = 25$ mN m^{-1} (*open circles*), 40 mN m^{-1} (*triangles*), and 55 mN m^{-1} (*filled circles*); and for simulations conducted at selected, single helix tilt angles (*solid lines*) and simulations using linear combinations of two different pairs of helix tilt angles (*dashed lines*) as noted. The *inset* shows the simulated dichroic ratio dependence on incident angle for helix tilt angles of 5° and 25°

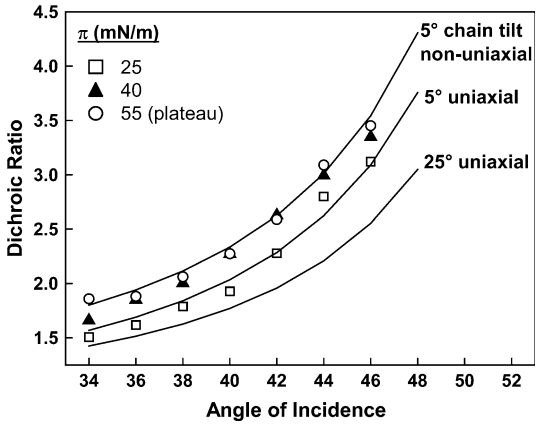

Fig. 6 Dichroic ratio of the asymmetric CH_2 stretching band intensity as a function of angle of incidence for IRRAS compression mode experiments conducted at $\pi = 25$ mN m^{-1} (*squares*), 40 mN m^{-1} (*triangles*), and 55 mN m^{-1} (*circles*). Best-fit simulated lines were generated using an acyl chain tilt of 5° and a uniaxial (fit to data acquired at $\pi = 25$ mN m^{-1}) or nonuniaxial (fit to data acquired at $\pi = 40$ and 55 mN m^{-1}) chain distribution. A simulated curve using a uniaxial distribution and a chain tilt of 25° is also shown for comparison

more appropriate for this system, for the following reasons:

1. The AFM data (Fig. 3d) clearly reveal the presence of both monolayers and multilayers in this system at a surface pressure of 55 mN m^{-1}.
2. It is known from previous (bulk phase) ATR studies (Pastrana et al. 1991) that the tilt of the SP-C helix in bilayers is approximately parallel to the acyl chains (i.e., approximately 25°) in DPPC multilayers.
3. As is evident from Fig. 5, the helix tilt angle is unchanged over a range of surface pressures from 25 to 40 mN m^{-1} in compression (vide supra). The latter value is as close to the plateau region as we can achieve experimentally while the film still remains in the monolayer state. Thus, there is no progressive decrease in helix tilt angle with increasing pressure in the absence of multilayers.
4. If the one-state model is assumed to be reasonable, then the helix tilt in the system must be the same for SP-C in monolayers as in bilayers. Since the helical region of SP-C is very hydrophobic, the helix should be tilted to match the hydrophobic thickness of the lipid acyl chains in both monolayers and bilayers. Thus, the orientation of the acyl chains in each state will determine the helix tilt. We have monitored the acyl chain tilt in the current system to test this idea. The results are shown in Fig. 6. The acyl chain tilt was determined as previously discussed (Brauner et al. 2003; Flach et al. 2001) from intensity measurements of the asymmetric CH_2 stretching vibration at surface pressures of 25, 40 and 55 mN m^{-1}. In each case, the frequency of this band ($2{,}919 \pm 0.5$ cm^{-1}) indicated essentially all-*trans* conformational order in the acyl chains and the experimental data were best fit using a 5° chain tilt. It is interesting to note that to fit the data at the higher two pressures, slight nonuniaxial symmetry (Brauner et al. 2003) was required. In any case, our observation is that the acyl chains are essentially perpendicular to the aqueous surface at each pressure. This is incompatible with the idea that helix tilt in the system must be the same for SP-C in monolayers as in bilayers. Simply stated, to match the lipid hydrophobic thickness in monolayers the protein helix must be much more highly tilted than it is in bilayers.

Overall, all lines of evidence suggest that a two-state model is a more reasonable way to explain the high-pressure IRRAS data. For quantitative analysis of the 55-mN-m^{-1} data in Fig. 5, two pieces of information are required, namely SP-C tilt in monolayers and in bilayers. The current study (monolayers at $\pi = 25$ or 40 mN m^{-1}) has determined the former to be 80°, while the tilt in bilayers has been measured at 25°. It is reasonable to alternatively assume that packing considerations in bilayers would lead to the approximate matching of the protein tilt with the chain tilt (i.e., 5°). Since we cannot distinguish between these two possibilities for SP-C tilt in multilayers, we carried out the calculations shown in Fig. 5 both ways. We assume the observed (overall average) helix tilt arises from a fraction of the protein molecules (in monolayers) tilted at 80° and a fraction (in bilayers) tilted either at 5° or at 25°. The simulated data show that the best fit for each of these scenarios is ob-

tained for 85% of the SP-C helices tilted at 80° and 15% tilted at 5° or 70% of the SP-C helices tilted at 80° and 30% tilted at 25°. These simulated curves are included in Fig. 5 along with an inset that depicts the simulated ratios for helix tilts of 5° and 25°. The general conclusion is that 70–80% of the protein is distributed in the monolayer phase; the remainder is associated with bilayers.

Discussion

Recent advances in a variety of microscopic techniques have provided insight into the mechanics of pulmonary surfactant function. The detection of a surface-associated multilamellar phase formed during the compression of various lung surfactant model systems under physiologically relevant surface pressure conditions along with observations of similar phases in the alveolar surface film of a guinea pig lung (Schürch et al. 1998) have led to refinements in the squeeze-out hypothesis. In general terms, squeeze-out refers to the exclusion of relatively fluid lipid and protein from the monolayer into a surface-associated reservoir without complete exclusion of components into the aqueous subphase (Diemel et al. 2002b). The hydrophobic surfactant proteins SP-B and SP-C have each been observed to promote the formation of multilayers and an anionic PG lipid constituent appears to be essential as well (Bourdos et al. 2000; Diemel et al. 2002b). In terms of the composition of the multilamellar stacks, TOF-SIMS results of lipid/SP-C model systems have revealed that the excluded material is enriched in SP-C and also contains some DPPC, contrary to early squeeze-out descriptions where DPPC was assumed to remain at the interface within the monolayer (Bourdos et al. 2000; Galla et al. 1998). Respreading or readsorption of surfactant from the reservoir to the air/alveolar interface has been suggested as a mechanism to maintain a continuous surface film and to provide alveolar stability during inhalation. Although significant advances have been made, no information is available about the molecular structure modifications that accompany the exclusion and reinsertion process.

In the current study, we have used the nanoscale sensitivity of AFM to verify that multilayer formation in the DPPC/DPPG/cholesterol surfactant model system is dependent on the presence of SP-C. In addition, IRRAS experiments have revealed important molecular structure and orientation information pertaining to SP-C in both monolayer and mixed monolayer/multilayer environments. The AFM image and line plot shown in Fig. 3d provide compelling evidence that multilayer formation does indeed take place in the presence of SP-C within the plateau region of the isotherm shown in Fig. 2. Thus, the AFM results provide us with the context (monolayer or bilayer) in which to discuss the SP-C helix orientation information obtained from the IRRAS experiments conducted at the two different pressure values. We will first compare the isotherms and AFM results for the model system used in the current study with previously reported work on similar systems, followed by discussion and integration of the IRRAS results with published molecular structure and orientation information from monolayer and bulk phase environments. Finally, a schematic model for the exclusion and respreading process will be presented.

The current experiments were conducted on a mixture of DPPC/DPPG (4/1 mol/mol) with 7 mol% cholesterol in the presence and absence of 4 mol% native porcine SP-C. The relative concentration of the two phospholipid headgroups in the mixture is similar to that found in a variety of mammalian surfactants although the acyl chain distribution in the native systems varies significantly (Postle et al. 2001; Veldhuizen et al. 1998). The level of cholesterol added in the model system is based on that reported for human surfactant (Veldhuizen et al. 1998). The concentration of SP-C was kept as low as possible, consistent with adequate signal-to-noise levels in the Amide I band so that quantitative IRRAS simulations could be conducted.

Several similarities are noted on comparing the isotherms and the AFM topography for the model system used in this study in the presence of SP-C (Fig. 2) with those previously published for a system consisting of DPPC/DPPG/SP-C (4/1 mol/mol, 0.4 mol% SP-C) (von Nahmen et al. 1997). Most important is the initiation of the plateau in the isotherms observed at $\pi \sim 55$ mN m^{-1} for both systems. In addition, the AFM images for LB films transferred in the plateau region for the two systems reveal a similar network structure for the protrusions. These observations indicate that multilayer formation for this lipid mixture proceeds independent of the presence of cholesterol and for a fairly wide range of SP-C concentration.

More recent studies have specifically explored the effect of cholesterol on surface activity and surface topography for a model SP-C-containing system (Diemel et al. 2002a). The system was quite similar in SP-C (3 mol%) and cholesterol (10 mol%) concentration, but differed significantly in the lipid acyl chain content (DPPC/1-palmitoyl-2-oleoyl phosphatidylcholine/POPG, 50/30/20 mol) compared with that used in the current set of experiments. For the films containing unsaturated lipids, a small plateau indicative of squeeze-out was observed at a surface tension of 27 mN m^{-1} ($\pi = 45$ mN m^{-1}) only in the presence of cholesterol. The AFM topography of a cholesterol-containing LB film transferred at a surface tension of 22 mN m^{-1} ($\pi = 50$ mN m^{-1}) shows a well-dispersed population of nearly circular protrusions. Comparisons with the current AFM topography (Fig. 3d) indicate that unsaturation in the lipid acyl chains has a significant effect on the distribution of the protrusions in the plane of the film, most likely a reflection of differences in the fluidity of the phases present prior to the initiation of the squeeze-out process (the phase behavior of various surfactant models in monolayers has been recently reviewed (Piknova et al. 2002)). Differences are also observed in

protrusion height where multilayers of predominantly approximately 4 and 8 nm in height are detected for the unsaturated system (Diemel et al. 2002a) versus a larger distribution of heights in multiples of approximately 4 nm for the current system as shown in Fig. 3d. We are hesitant to suggest that the height differences of the protrusions arise from the variations in lipid chain saturation, since height has been found to be highly dependent on the experimental protocol used in transferring LB films.

The position of the Amide I band at approximately 1,650 cm^{-1} in the IRRAS spectra shown in Fig. 4 indicates that the predominant conformation of the protein is helical in both monolayer and multilamellar environments. This is consistent with previously reported IRRAS results for DPPC/SP-C monolayers (Gericke et al. 1997) and with ATR IR spectra for DPPC/DPPG or egg PG/SP-C multilayer films (Pastrana et al. 1991; Vandenbussche et al. 1992). The small increase in the frequency of the Amide I band observed in the current studies when IRRAS spectra are acquired at the higher pressure value may be due to a slight increase in the α-helical content in a bilayer versus a monolayer environment. The increase in frequency may also result from an increase in the hydrophobicity of the environment near the N-terminal segment of the helical portion in the multilayer compared with the monolayer phase. The dominant Amide I component reported for SP-C reconstituted in lipid vesicles, i.e., a hydrophobic environment, was 1,656 cm^{-1} (Pastrana et al. 1991), whereas band components at lower frequencies (approximately 1,635 cm^{-1}) have been assigned to a hydrated α-helical structure for other peptides (Martinez and Millhauser 1995; Williams et al. 1996), including a peptide based on the N-terminus of SP-C (Bi et al. 2002).

An evaluation of the IRRAS Amide I band intensities suggests that the helix tilt angle adapts to the thickness of the lipid acyl chain region in monolayers and bilayers. More specifically, a helix tilt angle of 80° was found in monolayers at $\pi = 25$ and 40 mN m^{-1} (in the compression mode), while the data acquired at $\pi = 55$ mN m^{-1} seem best evaluated considering the presence of the two different lamellar states, i.e., monolayers and bilayers. Considering the dimensions of the AFM image shown in Fig. 3d (10×10 μm^2) and the macroscopic size of the IR beam (approximately 2–4-mm diameter), it is clear that spectral acquisition occurs over a region containing both monolayers and monolayer/multilayer domains (at high pressure). The depth of sampling by the IR beam is estimated to be approximately 400–500 nm (Kudryashova et al. 2003), which more than encompasses the height of the protrusions measured by AFM. Accordingly, our use of the two-state model seems appropriate. The calculated orientation results lead to the interpretation that within the area sampled by the IR beam, 70–80% of the SP-C resides in a monolayer, while the remainder is located in multilamellar stacks. At this point, however, we are unable to determine whether the relative concentration of SP-C is enhanced in the multilayer regions owing to the inhomogeneous distribution of the protrusions as shown in the AFM image (Fig. 3d) and the fact that the distribution of phases within the particular area sampled by the IR beam cannot be determined. One important observation is that the helix tilt angles in both phases allow for near optimal hydrophobic matching between the helical region of the protein and the lipid acyl chains.

Essentially complete reinsertion of the reservoir into the monolayer upon film expansion in the presence of SP-C is evident from the retracing of the original isotherm during subsequent compression (Fig. 2). This is attributed to the proximity of the excluded material to the interface and the presence of SP-C. Reports from both epifluorescence microscopy of monolayers and AFM of LB films demonstrate that the appearance of various lipid/SP-C films after compression and expansion to low pressure closely resemble the film during initial compression (Pérez-Gil and Keough 1998). It is of interest to note in the current IRRAS experiments conducted in the expansion mode at $\pi = 25$ mN m^{-1} that the orientation of the helices (one-state model) or the relative amount of SP-C in the monolayer versus the multilayer phase (two-state model) depends upon the extent of compression in the plateau region. Typical effects are noted in Fig. 7. Two data sets for expanded films acquired at $\pi \sim 25$ mN m^{-1} are depicted in the figure. The data represented by open circles were obtained from a sample where the isotherm had a plateau length of approximately 14 $Å^2$ per molecule, while the data represented by the closed circles are from a sample with a plateau length of approximately 30 $Å^2$ per molecule. Simulations that best fit the data using the one-

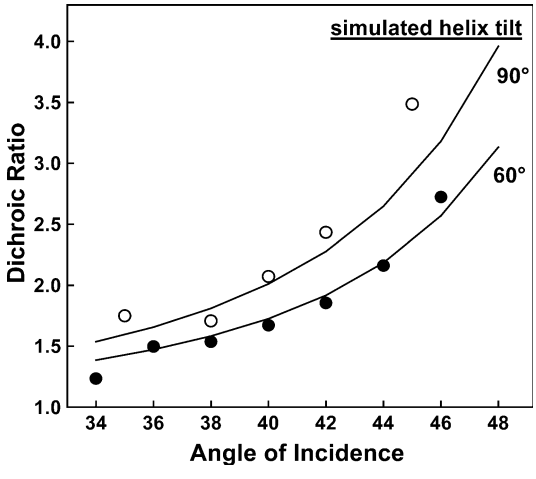

Fig. 7 Dependence of helix orientation on the extent of film compression determined by fitting measured dichroic ratios obtained from IRRAS expansion mode experiments at $\pi = 25$ mN m^{-1} with simulated curves. Amide I band intensity ratios obtained from films where the isotherm plateau length was approximately 14 $Å^2$ per lipid molecule (*open circles*) are best fit using a helix tilt angle of 90° and data from samples with a plateau length of approximately 30 $Å^2$ per lipid molecule (*filled circles*) are fit with simulations using a 60° helix tilt

state model in each case (also shown in Fig. 7) are conducted using considerably different tilt angles. Alternatively, when the experimental dichroic ratios are evaluated using the two-state model, a higher proportion of multilayer compared with monolayer phase is indicated for the film undergoing a higher degree of compression.

Overall, these results provide some evidence for the transport of SP-C between monolayer and multilayer phases. We speculate that the changes in helix orientation upon compression and subsequent expansion coupled with the hydrophobic interaction between the amino acid side chains and the lipid acyl chains facilitates the movement and reorganization of surfactant components between the monolayer and multilamellar states.

A schematic model depicting the orientation of the helical portion, as derived in the current experiments, and possible locations for the two palmitoyl chains of SP-C in monolayer and multilamellar environments is shown in Fig. 8. Similar models have been previously published (Galla et al. 1998; Pérez-Gil and Keough 1998). The palmitoyl chains of SP-C are shown inserted in the same leaflet as the helical portion and bridging opposing monolayer-to-bilayer and bilayer-to-bilayer structures. The bridging is suggested to promote close monolayer–bilayer and bilayer–bilayer contacts through which the proximity of the reservoir to the monolayer is maintained. In this way, rapid respreading upon film expansion is facilitated. TOF-SIMS results provide evidence of SP-C enrichment in the multilayers (Bourdos et al. 2000; Galla et al. 1998), which is likely to promote DPPG enrichment as well, since an electrostatic interaction exists between the PG headgroup and the positively charged N-terminus of SP-C. Consequently, the DPPG content in the multilayer portion of the illustration is enhanced. The figure also depicts the presence of DPPC in the multilamellar stacks consistent with earlier reports (Bourdos et al. 2000; Galla et al. 1998).

The current IRRAS results provide the first evidence obtained in situ, i.e., at the A/W interface, of the change in helix tilt angle of SP-C accompanying the monolayer-to-multilayer transition. Although care must be taken when results are extrapolated to the full complement of pulmonary surfactant constituents at the air/alveolar lining, comparison of the current AFM results with several model systems along with the molecular-level information obtained by IRRAS yields a consistent picture for the role of SP-C in the exclusion and reinsertion process. Investigations providing molecular structure and orientation information pertinent to the function of pulmonary surfactant protein SP-B, related peptides, and anionic and unsaturated lipid constituents are continuing.

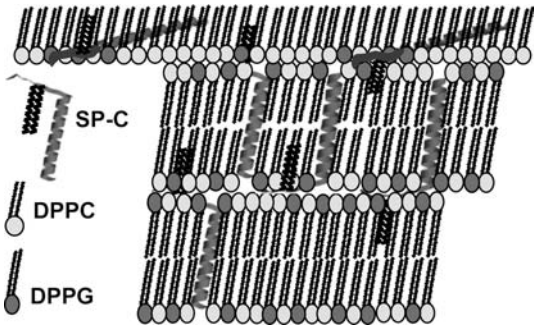

Fig. 8 Simplified model of DPPC/DPPG/SP-C monolayer/multilayer structures formed at the air/water interface in the plateau region of the isotherm, based on the helix tilt angles suggested by the current IRRAS measurements

Acknowledgements This work was supported by PHS grant GM 29864 to R.M.

References

Bertie JE, Ahmed MK, Eysel HH (1989) Infrared intensities of liquids. 5. Optical and dielectric constants, integrated intensities, and dipole moment derivatives of H_2O and D_2O at 22°C. J Phys Chem 93:2210–2218

Bi X, Flach CR, Perez-Gil J, Plasencia I, Andreu D, Oliveira E, Mendelsohn R (2002) Secondary structure and lipid interactions of the N-terminal segment of pulmonary surfactant SP-C in Langmuir films: IR reflection-absorption spectroscopy and surface pressure studies. Biochemistry 41:8385–8395

Bourdos N, Kollmer F, Benninghoven A, Ross M, Siever M, Galla H-J (2000) Analysis of lung surfactant model systems with time-of-flight secondary ion mass spectrometry. Biophys J 79:357–369

Brauner JW, Flach CR, Xu Z, Bi X, Lewis RNAH, McElhaney RN, Gericke A, Mendelsohn R (2003) Quantitative functional group orientation in Langmuir films by infrared reflection-absorption spectroscopy: C = O groups on behenic acid methyl ester and *sn*2−^{13} C-DSPC. J Phys Chem B 107:7202–7211

Diemel RV, Snel MME, van Golde LMG, Putz G, Haagsman HP, Batenburg JJ (2002a) Effects of cholesterol on surface activity and surface topography of spread surfactant films. Biochemistry 41:15007–15016

Diemel RV, Snel MME, Waring AJ, Walther FJ, van Golde LMG, Putz G, Haagsman HP, Batenburg JJ (2002b) Multilayer formation upon compression of surfactant monolayers depends on protein concentration as well as lipid composition. J Biol Chem 277:21179–21188

Flach CR, Gericke A, Mendelsohn R (1997) Quantitative determination of molecular chain tilt angles in monolayer films at the air/water interface—infrared reflection/absorption spectroscopy of behenic acid methyl ester. J Phys Chem B 101:58–65

Flach CR, Xu Z, Bi X, Brauner JW, Mendelsohn R (2001) Improved IRRAS apparatus for studies of aqueous monolayer films: determination of the orientation of each chain in a fatty-acid homologous Ceramide 2. Appl Spectrosc 55:1060–1066

Fraser RDB, MacRae TP (1973) Conformation in fibrous proteins and related synthetic polypeptides. Academic, New York

Galla H-J, Bourdos N, von Nahmen A, Amrein M, Sieber M (1998) The role of pulmonary surfactant protein C during the breathing cycle. Thin Solid Films 329:632–635

Gericke A, Flach CR, Mendelsohn R (1997) Structure and orientation of lung surfactant SP-C and L-a-dipalmitoylphosphatidylcholine in aqueous monolayers. Biophys J 73:492–499

Glasser SW, Burhans MS, Korfhagen TR, Na C-L, Sly PD, Ross GF, Ikegami M, Whitsett JA (2001) Altered stability of pulmonary surfactant in SP-C-deficient mice. Proc Natl Acad Sci U S A 98:6366–6371

Goerke J, Clements JA (1986) Alveolar surface tension and lung surfactant. In: Mackelm PT, Mead J (eds) Handbook of physiology: the respiratory system III. American Physiology Society, Washington, pp 247–261

Johansson J, Szyperski T, Curstedt T, Wuthrich K (1994) The NMR structure of the pulmonary surfactant-associated polypeptide SP-C in an apolar solvent contains a Valyl-rich Alpha-Helix. Biochemistry 33:6015–6023

Knebel D, Sieber M, Reichelt R, Galla H-J, Amrein M (2002) Scanning force microscopy at the air-water interface of an air bubble coated with pulmonary surfactant. Biophys J 82:474–480

Krol S, Ross M, Sieber M, Künneke S, Galla H-J, Janshoff A (2000) Formation of three-dimensional protein-lipid aggregates in monolayer films induced by surfactant protein B. Biophys J 79:904–918

Kudryashova EV, Meinders MBJ, Visser AJWG, van Hoek A, de Jongh HHJ (2003) Structure and dynamics of egg white ovalbumin adsorbed at the air/water interface. Eur Biophys J 32:553–562

Kuzmin VL, Michailov AV (1981) Molecular theory of light reflection and applicability limits of the macroscopic approach. Opt Spectrosc (USSR) 51:383–385

Kuzmin VL, Romanov VP, Michailov AV (1992) Reflection of light at the boundary of liquid systems and structure of the surface layer: a review. Opt Spectrosc 73:1–26 [translated from Opt Spektrosk (1992) 73, 3–47]

Marsh D (1990) CRC Handbook of Lipid Bilayers. CRC Press, Boca Raton

Martinez G, Millhauser G (1995) FTIR spectroscopy of alanine-based peptides: assignment of the Amide I' modes for random coil and helix. J Struct Biol 114:23–27

Mendelsohn R, Liang GL, Strauss HL, Snyder RG (1995) IR spectroscopic determination of gel state miscibility in long-chain phosphatidylcholine mixtures. Biophys J 69:1987–1998

von Nahmen A, Schenk M, Sieber M, Amrein M (1997) The structure of a model pulmonary surfactant as revealed by scanning force microscopy. Biophys J 72:463–469

Pastrana B, Mautone AJ, Mendelsohn R (1991) Fourier transform infrared studies of secondary structure and orientation of pulmonary surfactant SP-C and its effect on the dynamic surface properties of phospholipids. Biochemistry 30:10058–10064

Pastrana-Rios B, Flach CR, Brauner JW, Mautone AJ, Mendelsohn R (1994) A direct test of the "squeeze-out" hypothesis of lung surfactant function—external reflection FT-IR at the air/water interface. Biochemistry 33:5121–5127

Pérez-Gil J, Keough KMW (1998) Interfacial properties of surfactant proteins. Biochim Biophys Acta 1408:203–217

Piknova B, Schram V, Hall SB (2002) Pulmonary surfactant: phase behavior and function. Curr Opin Struct Biol 12:487–494

Plasencia I, Cruz A, Casals C, Pérez-Gil J (2001) Superficial disposition of the N-terminal region of the surfactant protein SP-C and the absence of specific SP-B—SP-C interactions in phospholipid bilayers. Biochem J 359:651–659

Postle AD, Heeley EL, Wilton DC (2001) A comparison of the molecular species compositions of mammalian lung surfactant phospholipids. Comp Biochem Physiol A Physiol 129:65–73

Rothschild KJ, Clark NA (1979) Polarized infrared spectroscopy of oriented purple membrane. Biophys J 25:473–488

Schürch S, Green FHY, Bachofen H (1998) Formation and structure of surface films: captive bubble surfactometry. Biochim Biophys Acta 1408:180–202

Takamoto DY, Lipp MM, van Nahmen A, Lee KYC, Waring AJ, Zasadzinski JA (2001) Interaction of lung surfactant proteins with anionic phospholipids. Biophys J 81:153–169

Vandenbussche G, Clercx A, Curstedt T, Johansson J, Jörnvall H, Ruysschaert JM (1992) Structure and orientation of the surfactant-associated protein C in a lipid bilayer. Eur J Biochem 203:201–209

Veldhuizen R, Nag K, Orgeig S, Possmayer F (1998) The role of lipids in pulmonary surfactant. Biochim Biophys Acta 1408:90–108

Williams S, Causgrove TP, Gilmanshin R, Fang KS, Callender RH, Woodruff WH, Dyer RB (1996) Fast events in protein folding: helix melting and formation in a small peptide. Biochemistry 35:691–697